

## **Visualizations of viscoelastic flow in a 4:1 square/square contraction**

by

M. A. Alves

Departamento de Engenharia Química, CEFT, Faculdade de Engenharia, Universidade do Porto  
Rua Dr. Roberto Frias s/n, 4200-465 Porto, Portugal, mmalves@fe.up.pt

F. T. Pinho

Centro de Estudos de Fenómenos de Transporte, DEM, Escola de Engenharia, Universidade do Minho  
Campus de Azurém, 4800-058 Guimarães, Portugal, fpinho@dem.uminho.pt

P. J. Oliveira

Departamento de Engenharia Electromecânica, Universidade da Beira Interior  
6201-001 Covilhã, Portugal, pjpo@ubi.pt

### **ABSTRACT**

Visualizations of the three-dimensional flow in a 4:1 square-square sudden contraction were carried out for a Newtonian and two viscoelastic fluids under conditions of negligible inertia. In the case of the Newtonian fluid the influence of inertia was also studied, and it was found that for Reynolds numbers above 0.1 a significant decrease of the recirculation is observed. In the case of viscoelastic fluids increasing the flowrate leads to different flow patterns depending on the Deborah number and the type of viscoelastic fluid: whereas for the Boger fluid a complex flow pattern was observed, with a decrease on the vortex size up to Deborah numbers of 0.2, followed by a moderate increase up to Deborah values of 0.8, for the shear-thinning viscoelastic fluid a dramatic increase on the size of the vortex was observed. With both viscoelastic fluids an elastic instability leads to the onset of a periodic flow at high flow rates, but in both cases under conditions of negligible inertia. For the shear-thinning viscoelastic the periodic flow was characterized by a constant Strouhal number of 0.5. In the steady flow regime the vortices are not closed and fluid particles enter the middle-plane vortex, rotate towards its eye, drift to the diagonal-plane vortex, then rotate to its periphery and exit to the downstream duct, a dynamic process that is opposite that observed and predicted numerically for Newtonian fluids.

## 1. INTRODUCTION

Sudden contraction flows are classical benchmark problems used in computational rheology (Hassager, 1988), and a large number of visualization studies in planar and axisymmetric contractions with various non-Newtonian fluids are reported in the literature (Boger and Walters, 1993). The flow behaviour of non-Newtonian fluids in this simple configuration can be very surprising, and different flow patterns are observed even for fluids with apparently similar rheological behaviour.

The first visualizations with viscoelastic fluids were carried out by Cable and Boger (1978a, 1978b, 1979) and Nguyen and Boger (1979) for contraction ratios in the range 7.67:1 to 14.83:1, who reported a dramatic growth of the salient corner vortex for shear rates higher than the critical value above which the first normal stress difference grew quadratically. At much higher Weissenberg numbers, a measure of flow elasticity given by the ratio of fluid to flow characteristic times, the flow became asymmetric and eventually time-dependent. In 1986 Boger et al investigated the behaviour of Boger fluids (viscoelastic fluids with a constant shear viscosity) having similar steady and dynamic shear properties and yet found different vortex dynamics: they concluded that a different fluid property had to be taken into account and, in his 1987 review paper, Boger suggested extensional viscosity as that property. For some fluids only a corner vortex exists, which grows in size as elasticity increases, whereas for other fluids the corner vortex extends to the re-entrant corner near which a lip vortex forms. For high contraction ratios, the two vortices are initially separate, but separated vortices were also seen by McKinley et al (1991) in 4:1 contraction experiments. As the elasticity increases the lip vortex grows at the expense of the corner vortex, while the length of the recirculation remains fairly constant.

Subsequently, the 4:1 planar and axisymmetric contractions became the focus of a variety of experimental and numerical works aimed at various objectives. The experimental work concentrated on the investigation of the various flow transitions and instabilities and used several experimental techniques, as in the case of McKinley et al (1991). The numerical simulations were unable to predict correctly the sub-critical steady flows and thus concentrated on improving the numerical techniques. The experiments of Walters and Webster (1982) and Evans and Walters (1986) found surprisingly different behaviours of Boger fluids in circular and planar contractions, and this has been recently confirmed by the experiments of Nigen and Walters (2002) for a variety of fluids: the same fluid shows increased pressure drop and vortex enhancement in axisymmetric contractions, but absence of vortex enhancement and the same pressure drop as the equivalent Newtonian fluid in planar contractions. An explanation for this was not given but it was shown that the extensional rate alone could not be the cause for the different behaviours.

Flow in square-square contractions has captured less attention and there are only a few experiments reported in the literature: Walters and Webster (1982) found similarities between flows through circular and square-square contractions, and this was confirmed by Walters and Rawlinson (1982) and Evans and Walters (1986) who suggested that vortex enhancement for Boger fluids in square-square contractions was as easy to achieve as in axisymmetric contractions. However, in the numerical experiments the geometry was somewhat different: a 2D planar contraction extending along the spanwise direction and 3D effects only due to the presence of end walls. Xue et al (1998) found vortex enhancement in this 3D planar contraction although the growth mechanism was different from that in other geometries, namely the lip vortex was absent. These simulations suggest the existence of some similarities with the flow in 2D axisymmetric contractions, but this clearly requires further investigation. In conclusion, three-dimensional contraction flows of viscoelastic fluids remain much less explored and promise new surprising features due to the added presence of transverse gradients of normal stress differences absent from the simpler two dimensional configurations. This is the motivation of the present work, which investigates experimentally some flow characteristics of the flow of well-controlled viscoelastic fluids under conditions of negligible inertia.

## 2. EXPERIMENTAL RIG

The experimental apparatus is schematically depicted in figure 1. It consists of two square ducts of length 1000 mm and 300 mm having sides of  $2H_1 = 24$  mm and  $2H_2 = 6$  mm, thus defining the 4:1 contraction ratio. Flow rate was set by an adequate control of applied pressure on the upstream duct and frictional losses in the long coiled pipe located at the bottom of the rig. To achieve low flow rates this coiled 8 m long pipe had a diameter of 4 mm, whereas for higher flow rates a larger 6 mm diameter pipe was used. Applied pressure was kept between 0.5 and 4 bar and the dashed lines in figure 1(a) represent lines of pressurised air. The flow rate was measured by a stopwatch and the passage of the liquid free-surface at two marks in the upper duct. In all tests the fluid temperature was measured and the fluid properties were taken from rheometric master curves.

Figure 1(b) illustrates the technique used to visualise the flow: the beam from a 10 mW He-Ne laser light source passed through a cylindrical lens to generate a sheet of light illuminating highly reflective tracer particles suspended

in the fluid (circa 15 mg/kg fluid of PVC particles with 10  $\mu\text{m}$  diameter). Their trajectories were recorded using long time exposure photography with a conventional camera (Canon EOS300 with a macro EF100 mm f/2.8 lens).

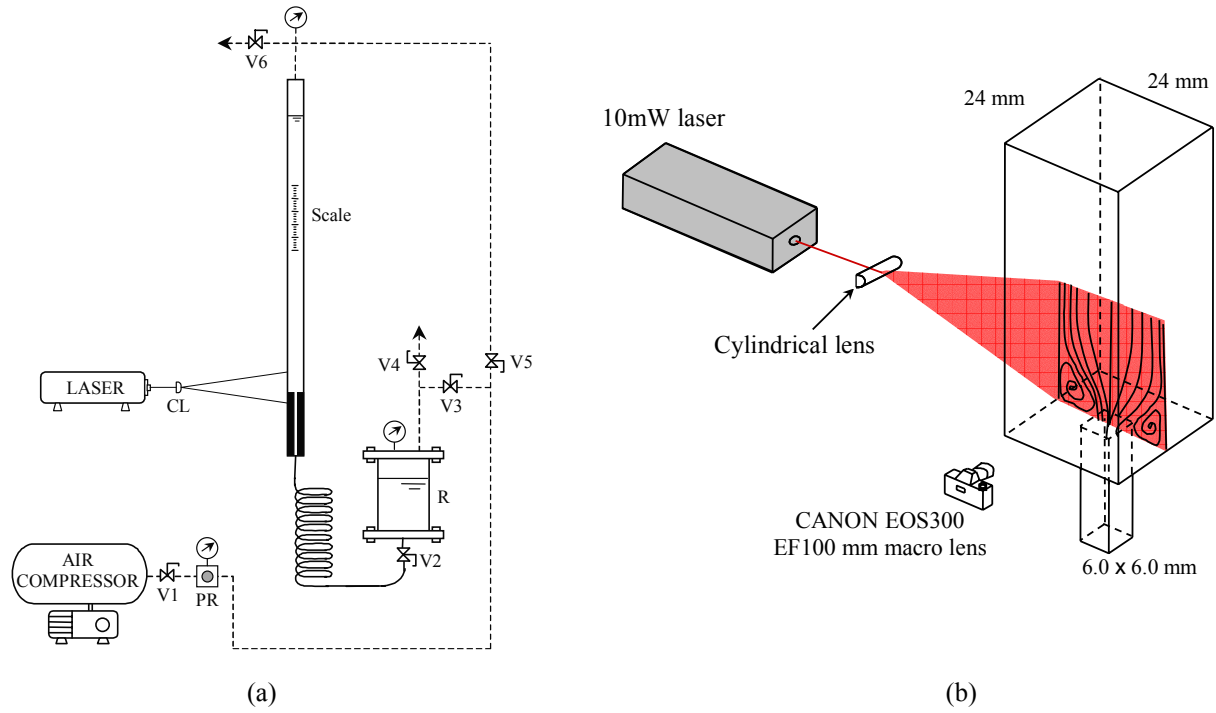


Fig. 1. Experimental flow rig.

- a) Schematic representation of rig (PR - pressure regulator; V1 to V6 - ball valves; R- reservoir; CL - cylindrical lens)  
b) Flow visualization technique and test section.

### 3. RHEOLOGICAL CHARACTERISATION OF THE FLUIDS

The rheological properties of the viscoelastic fluids were measured by an AR2000 rheometer from TA Instruments with a cone-plate geometry, which could measure the shear viscosity ( $\eta$ ) and the first normal stress difference coefficient ( $\Psi_1$ ) in steady shear flow, and the rigidity and loss moduli ( $G'$ ,  $G''$ ) in dynamic shear flow.

Three fluids were investigated in this study: a viscous Newtonian fluid (N91), a Boger fluid (PAA100) and a shear-thinning viscoelastic fluid (PAA500) in order to illustrate the effect on the flow patterns of elasticity alone and in combination with shear-thinning. The composition of the fluids and some of their properties are shown in Table 1. To all solutions, 25 ppm of the biocide Kathon LXE from Rohm and Haas was added in order to reduce biological degradation of the fluids. The Boger fluid and the shear-thinning viscoelastic fluid are henceforth referred to as PAA100 and PAA500 fluids, respectively.

Table 1- Composition and properties of fluids (mass concentrations).

Designation	PAA [ppm]	Glycerine [%]	Water [%]	NaCl [%]	Kathon [ppm]	$\rho$ [ $\text{kg/m}^3$ ]	$\eta_0$ [Pa.s]
N91	-	90.99	7.51	1.50	25	1250	0.366
PAA100	100	90.99	7.50	1.50	25	1249	0.520
PAA500	500	84.97	14.98	-	25	1226	4.07

The effect of temperature on the shear properties is well predicted by an Arrhenius equation, with the shift factor defined as in Bird et al (1987)

$$\ln(a_T) = \ln\left(\frac{\eta}{\eta_0}\right) = \left[\frac{\Delta H}{R}\left(\frac{1}{T} - \frac{1}{T_0}\right)\right] \quad (1)$$

where  $\eta_0$  designates the zero-shear viscosity at the reference absolute temperature  $T_0$  ( $T_0 = 293.15$  K for PAA100 fluid and  $T_0 = 288.15$  K for PAA500 fluid), and the fitting of this equation to the experimental data gave  $\Delta H/R = 6860$  K for fluids N91 and PAA100 and  $\Delta H/R = 5900$  K for fluid PAA500.

The reduced rheological quantities (subscript  $r$ ) thus become those defined in Eq. (2)

$$\begin{aligned} \omega_r &\equiv \omega(T_0) = a_T \omega(T) & \dot{\gamma}_r &\equiv \dot{\gamma}(T_0) = a_T \dot{\gamma}(T) & G'_r &\equiv G'(T_0) = G'(T) & G''_r &\equiv G''(T_0) = G''(T) \\ \eta'_r &\equiv \eta'(T_0) = \eta'(T)/a_T & \eta''_r &\equiv \eta''(T_0) = \eta''(T)/a_T & \eta_r &\equiv \eta(T_0) = \eta(T)/a_T & \Psi_{1r} &\equiv \Psi_1(T_0) = \Psi_1(T)/a_T^2 \end{aligned} \quad (2)$$

Using these relations, the reduced steady shear data are plotted in figures 2 and 3 for the PAA100 and PAA500 fluids, respectively. Both figures included dynamic shear data in appropriate form in order to compare the corresponding limiting behaviours at vanishing deformations. The lines in the figures represent predictions by multi-mode constitutive models that were fitted to experimental data: a three-mode Oldroyd-B constitutive equation for the PAA100 and a four mode linear Phan-Thien—Tanner model for the PAA500 solution (with  $\varepsilon = 0.02$  and  $\xi = 0.04$ ). The parameters of the corresponding linear viscoelastic spectra are listed in Tables II.

Table 2- Linear viscoelastic spectra for the viscoelastic fluids ( $T_0 = 293.15$  K for PAA100 fluid;  $T_0 = 288.15$  K for PAA500 fluid).

Mode $k$	PAA100		PAA500	
	$\lambda_k$ [s]	$\eta_k$ [Pa.s]	$\lambda_k$ [s]	$\eta_k$ [Pa.s]
1	3.0	0.075	30.0	2.50
2	0.3	0.027	3.0	0.90
3	0.03	0.018	0.3	0.30
4	-	-	0.03	0.10
solvent	-	0.40	-	0.27

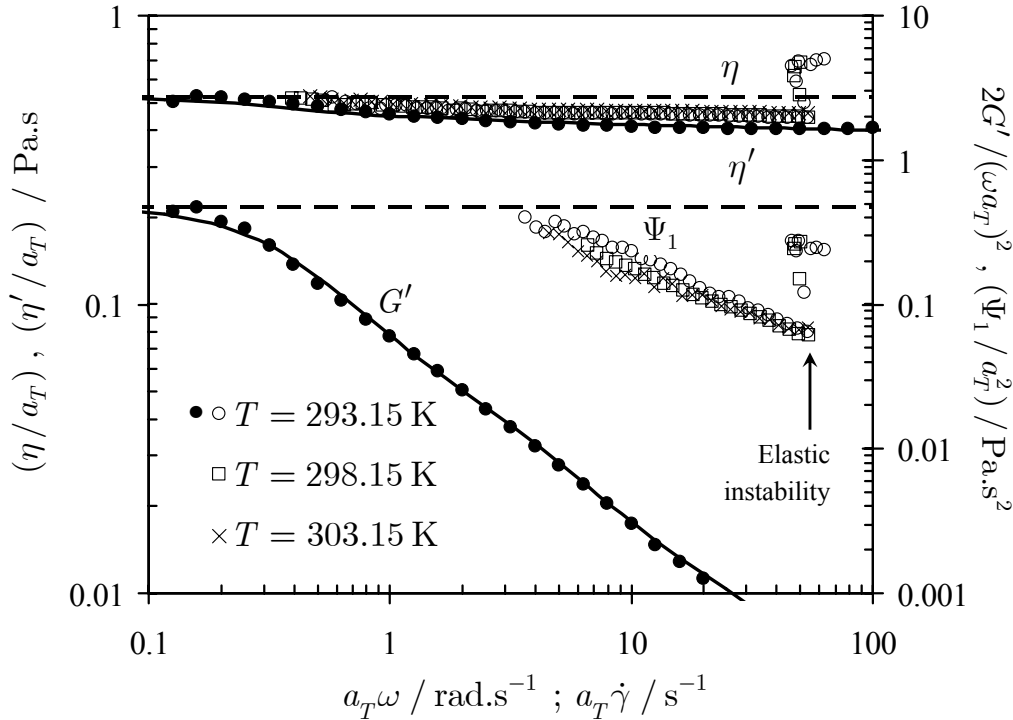


Fig. 2. Material parameters in steady ( $\eta$ ,  $\Psi_1$ ) and oscillatory ( $G'$ ,  $\eta'$ ) shear flow for the PAA 100 solution. Lines represent fitting by a three-mode Oldroyd-B model.

For the Boger fluid, the reduced shear viscosity is approximately constant at around 0.5 Pa.s in the reduced shear rate range of 0.3 to 50  $s^{-1}$  whereas the first normal stress coefficient exhibits a constant plateau at shear rates below 1  $s^{-1}$  and a shear-thinning behaviour elsewhere. The PAA500 is a mildly shear-thinning fluid: the decrease in the shear viscosity from the zero-shear rate viscosity to the infinite shear rate viscosity is by a factor of 10. At the



intermediate power law region the power law index has a value of around 0.46. In the measured range, the first normal stress difference coefficient is also shear-thinning, and a comparison between figures 3(a) and 3(b) shows the fluid to be highly elastic with  $N_1/(2\tau)$  increasing from around 3.5 at  $\dot{\gamma} = 1 \text{ s}^{-1}$  to around 6 at  $\dot{\gamma} = 100 \text{ s}^{-1}$ .

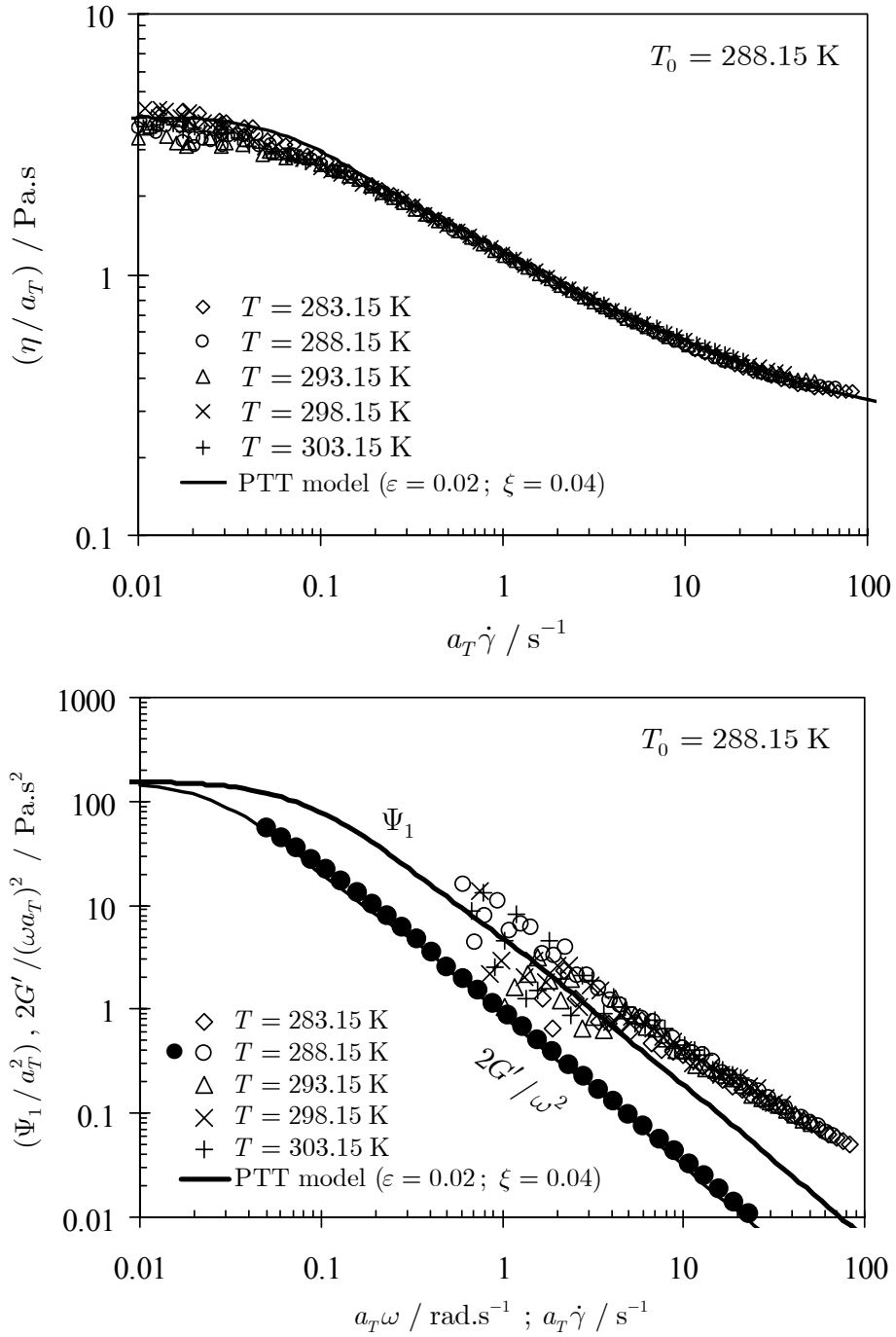


Fig. 3. Material parameters in steady ( $\eta, \Psi_1$ ) and oscillatory ( $G', \eta'$ ) shear flow for the PAA 500 solution. Lines represent fitting by a four-mode linear PTT model.

(a) Shear viscosity in steady shear

(b) First normal stress difference in steady shear and storage modulus in oscillating shear flow

#### 4. FLOW VISUALISATION RESULTS

#### 4.1. Newtonian fluid

Flow visualizations were carried out first with Newtonian fluids to assess the effect of inertia and to serve as a reference for comparison against the results for the viscoelastic fluids. For Newtonian fluids there is a reasonable amount of knowledge (Boger, 1987), although not for the square sudden contraction, and here comparisons were also carried out with results of numerical simulations. Figure 4 shows some pathlines for the flow of a Newtonian fluid in the middle plane of the 3D contraction and compares photographs with results of numerical simulations. The Reynolds number is defined as

$$Re_1 = \frac{\rho U_1 H_1}{\eta} \quad (3)$$

The vortex has a concave shape and, as expected, inertia leads to a reduction of its length especially for Reynolds numbers above 0.05 (Alves, 2004). As inertia becomes non-negligible the size of the vortices decrease with Reynolds number and eventually vanish at large flow rates. At low Reynolds numbers the dimensionless size of the middle-plane vortex is  $x_R/H_1 = 0.326$ , where  $H_1$  represents the upstream duct half-width. It is interesting to note that under creeping flow conditions the vortex size in a 4:1 circular contraction also asymptotes to exactly the same value. For the circular contraction Boger (1987) quotes a value of  $x_R/(2H_1) = 0.17 \pm 0.01$  based on experiments and simulations, in close agreement with our results.

Even though the flow inside the vortex looks two-dimensional, in reality it is three-dimensional and, in contrast to the planar and axisymmetric contractions, none of the recirculations are ever closed, as revealed by close inspection of the pathlines. In order to understand the descriptions of the Newtonian and non-Newtonian 3-D vortex flows let us consider two different vertical planes: the middle plane perpendicular to the wall (passing through points A-B, see figure 5), and always represented in the photos, and the second plane at  $45^\circ$  to the wall and passing through opposite corners of the square cross-section. In this second plane, henceforth referred as diagonal plane, no pictures were taken but the descriptions below result from visual inspection of the flow helped by results of the numerical simulations.

When the flow is Newtonian the fluid particles enter the vortex at the diagonal plane, rotate towards the centre of the diagonal-plane vortex and drift towards the eye of the middle-plane vortex. In the middle-plane vortex, particles rotate towards its periphery and exit the vortex at the re-entrant corner going into the downstream duct, thus giving the impression that in this plane this vortex is closed. The sketch of figure 5 helps to understand this description.

#### 4.2. Boger fluid

To quantify the strength of elastic effects it is convenient to use a single relaxation time in the definition of the Deborah number, which is expressed as

$$De_1 = \frac{\lambda_p(T) U_1}{H_1} = \frac{a_T \lambda_p(T_0) U_1}{H_1} \quad (4)$$

where  $\lambda_p$  is an equivalent relaxation time calculated from the linear viscoelastic spectrum of the fluid using the following equations:

$$\lambda_p = \sum_{k \neq \text{solvent}} \frac{\eta_k \lambda_k}{\eta_p} \quad \text{and} \quad \eta_p = \sum_{k \neq \text{solvent}} \eta_k \quad (5)$$

This definition guarantees that at low shear-rates the viscoelastic behaviour of the equivalent single mode model is identical to that of the multimode Oldroyd-B model. For the PAA100, the following values are obtained:  $\eta_0 \equiv \eta_s + \eta_p = 0.52$  Pa.s,  $\beta \equiv \eta_s/\eta_0 = 0.769$  and  $\lambda_p = 1.947$  s.

Streak photographs at the middle plane of the contraction are shown for the PAA100 fluid in figure 6 for increasing values of Deborah number. Now, the flow characteristics are complex and are mainly caused by elasticity because the Reynolds number is small ( $Re_1 < 0.11$ ). At low values of the Deborah number ( $De_1 = 0.041$ ), viscous effects predominate and the flow pattern is similar to that seen in figure 4 for Newtonian fluids, with the separation streakline still with a concave shape. With increasing Deborah number changes progressively occur: first, there is a very slight increase in vortex size while the separation streakline straightens, then the corner vortex progressively decreases in size to about a quarter at  $De_1 \approx 0.2$ , an effect not due to inertia since the Reynolds number remains lower than 0.05. McKinley et al (1991) reported results for a 4:1 axisymmetric contraction bearing some resemblance with the present ones: negligible elastic effects for  $De_2 < 1$  and a decrease in the corner vortex up to  $De_2 = 3.4$  (this Deborah number based on downstream flow quantities is related to ours by  $De_2 = 64De_1$ ).

However, in contrast to McKinley et al, the formation of a strong lip vortex, while the corner vortex decreases in size is not seen here, although the higher curvature of the streaklines at the reentrant corner suggests the possibility of a weak lip vortex (see photo for  $De_1=0.210$ ).

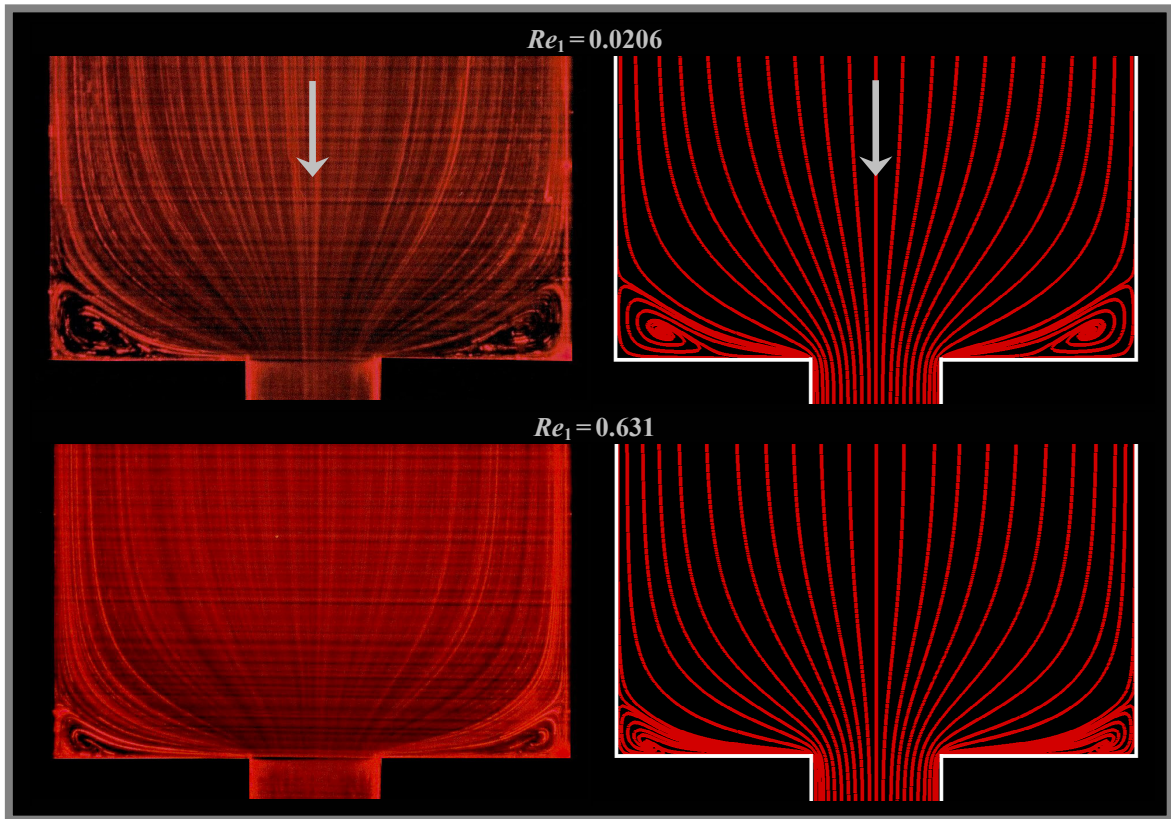


Fig. 4. Newtonian contraction flow in the middle plane under conditions of negligible inertia ( $Re_1=0.0206$ ) and for  $Re_1=0.631$ . Comparison with numerical results (right column).

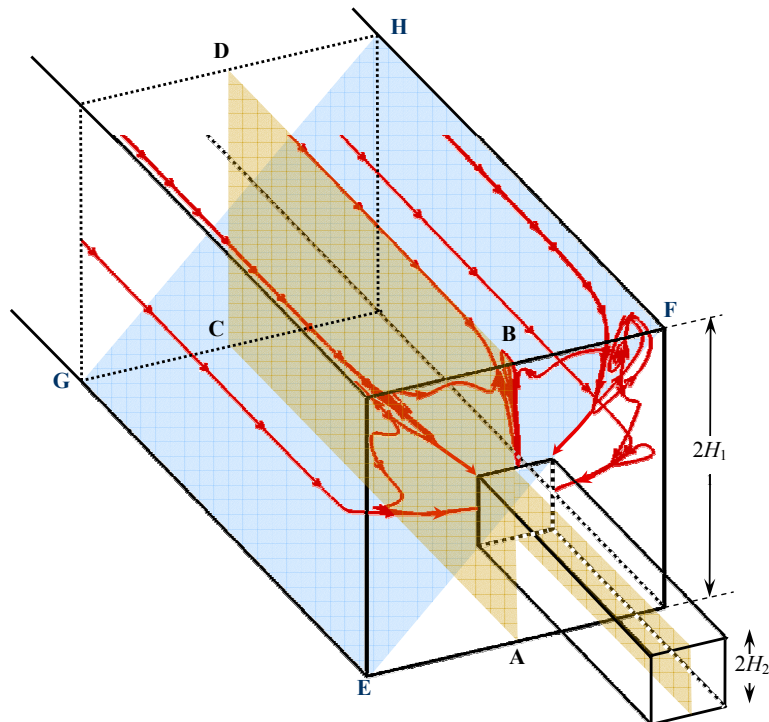


Fig. 5. Sketch of particle trajectories in the vortices for a Newtonian fluid under negligible inertia.

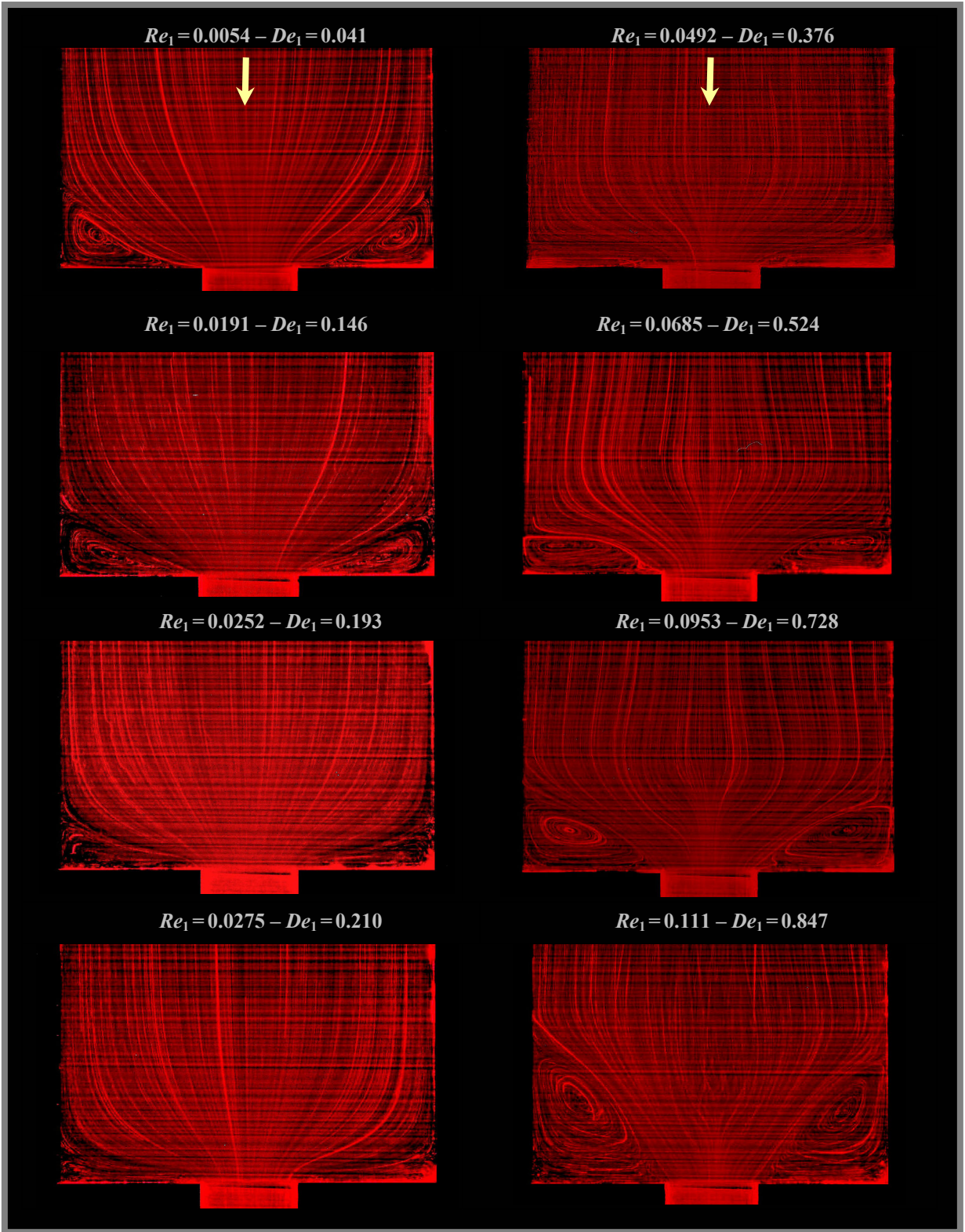


Fig. 6. Streaklines in the middle plane for the PAA100 at different flow rates.

As the Deborah number further increases the corner vortex starts to grow, and simultaneously changes occur in the characteristics of the streamlines approaching the contraction plane. For  $De_1 \geq 0.376$ , the approach flow streamlines in the middle plane progressively diverge with flow elasticity, an anomalous effect already predicted numerically by Alves et al (2000) for the flow of a Boger fluid in a 4:1 plane sudden contraction (see their figure 7 at  $De = 5$ ) and also observed by McKinley et al (1991) in their experiments with Boger fluids in circular



contractions. This upstream streamline divergence for Boger fluids can be attributed to a local intense increase in extensional viscosity leading to an increased flow resistance just upstream of the contraction plane as the extension rates grow in a region of predominantly extensional flow characteristics. This extensional thickening is characteristic of Boger fluids, but there are not enough data to correlate rheological behavior with diverging flow. The growth of a steady large vortex with elasticity continues up to  $De_1 \approx 0.8$ . Above this Deborah number the flow becomes periodic, possibly due to an elastic instability, as observed in the crossings of some streaklines for  $De_1 = 0.847$ . The amplitude of the oscillations increase with  $De_1$  and this can be seen in the three snap-shots of figure 7, taken at different moments within a cycle for one supercritical flow condition. At even higher flow rates the flow loses its periodicity.

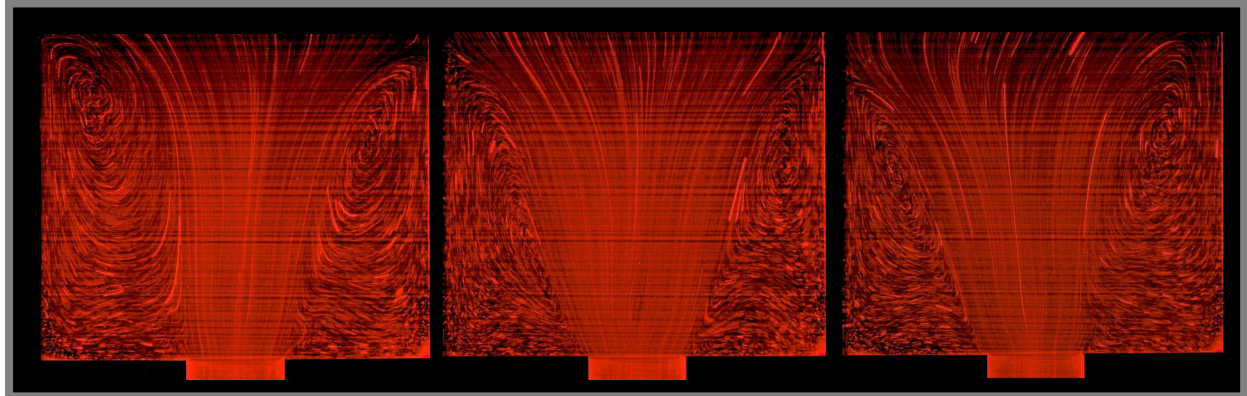


Fig. 7. Streaklines for the flow of PAA100 in the middle plane of a square-square contraction at three different moments within two different oscillating supercritical flow conditions ( $De_1=1.22$ ;  $Re_1=0.159$ ).

#### 4.3. Viscoelastic shear-thinning fluid

For the PAA500 fluid the following values were obtained from application of Eqs. (5) and (6) to the linear viscoelastic spectrum data:  $\eta_0 = \eta_s + \eta_p = 4.07$  Pa.s,  $\beta = \eta_s / \eta_0 = 0.0663$  and  $\lambda_p = 20.47$  s. Even though the characteristic shear rates in the actual flow fell outside the range of measured rheological data, the Deborah numbers could be calculated using this relaxation time ( $\lambda_p$ ).

For this fluid, the flow pattern variations previously identified with Boger fluids became more intense and dependent on the Deborah number, as can be inferred from figure 8. Two flow regimes are identified, both for conditions of negligible inertia: at low flow rates (Deborah numbers) the flow is steady, while at high flow rates it becomes unsteady but periodic. In all cases the flow is highly three-dimensional.

In the steady flow regime, represented by all photos in figure 8, we find the usual dramatic elastic vortex growth that is also present in plane and circular sudden contractions of shear-thinning viscoelastic fluids. At low flow rates (figure 8a) the 3-D flow pattern has some similarities to that for the Newtonian fluid, although the vortex has already a slightly different shape: it is neither convex nor concave, whereas for the Newtonian fluid in figure 4 the eddy has a clear concave shape. We can also see that the middle plane vortex appears to be closed. However, at higher flow rates (figures 8b to 8e), when the flow is dominated by fluid elasticity and the vortex is longer, the pictures suggest a second dramatic change in flow pattern.

At higher flow rates the direction of motion of fluid particles inside the vortices is opposite to that found at lower flow rates and with Newtonian fluids. This is more clearly suggested in figures 8(c) and 8(d): the fluid coming from the upstream duct enters the middle-plane vortex (see some of the white streaks), rotates towards its eye and then moves towards the eye of the diagonal-plane vortex where it rotates from the eye towards its periphery and exits the diagonal-plane vortex to the downstream duct (this was also confirmed by numerical simulations). This sequence was predicted numerically (Alves, 2004) and is illustrated in figure 9.

The important vortex growth is also seen in figure 10 which presents the variation of the normalised vortex length (of the middle plane vortex) with the upstream Deborah number. This figure includes data from the PAA100 Boger fluid and clearly shows that vortex growth is more intense with the shear-thinning fluid. At Deborah numbers in excess of 1.7, the flow of the PAA500 fluid becomes unsteady, but periodic.

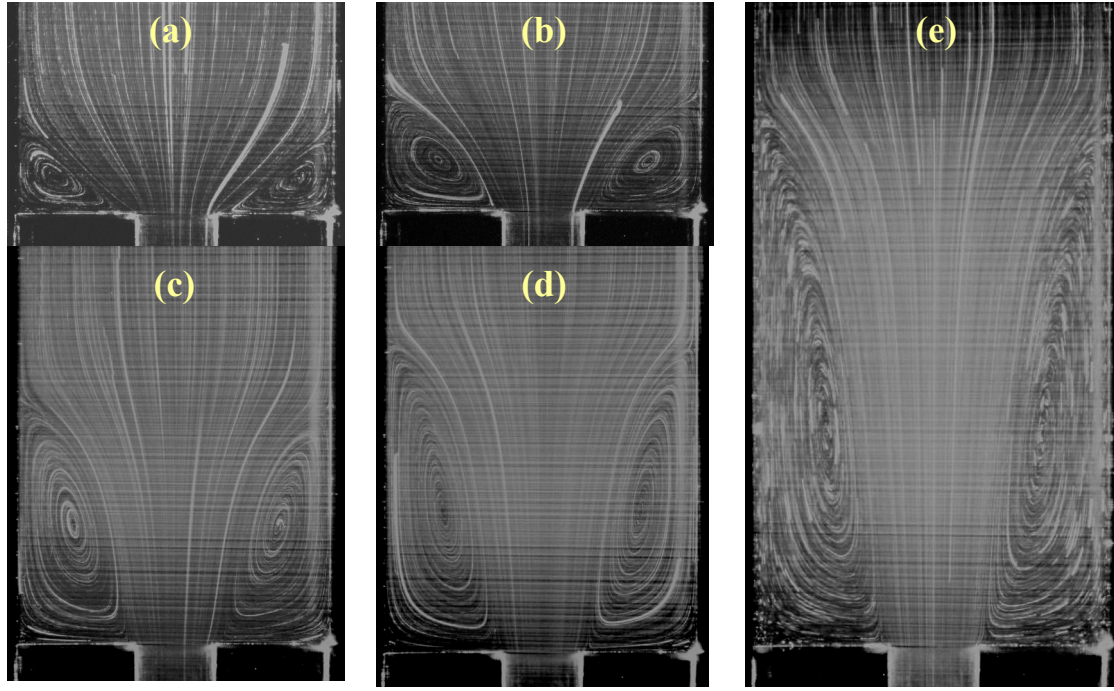


Fig. 8 - Corner vortex enhancement for fluid PAA500 in a 4:1 square/square contraction: (a)  $De_1=0.0241$ ; (b)  $De_1=0.0909$ ; (c)  $De_1=0.355$ ; (d)  $De_1=0.652$ ; (e)  $De_1=1.34$ .

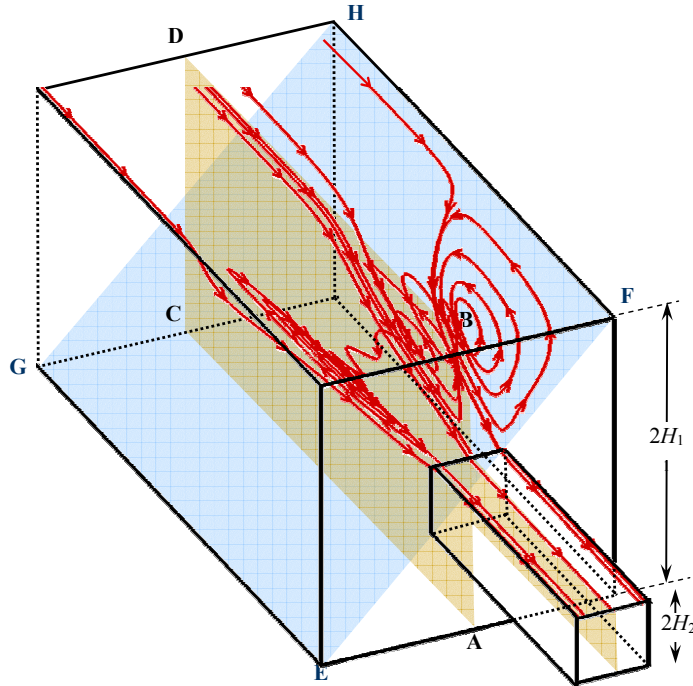


Fig. 9. Sketch of particle trajectories in the vortices for the PAA500 fluid under conditions of negligible inertia.

The sequence of photos in figure 11 represents three different moments within a cycle of flow periodicity for the PAA500 fluid. Obviously, those oscillations are occurring in both transverse directions. From films taken with a movie camera at a known frame rate it was possible to measure the frequency ( $f$ ) of oscillation for different flow rates within the periodic regime and a linear variation was found between these quantities, defining a constant Strouhal number  $St = 2fH_1/U_1 \approx 0.5$ .

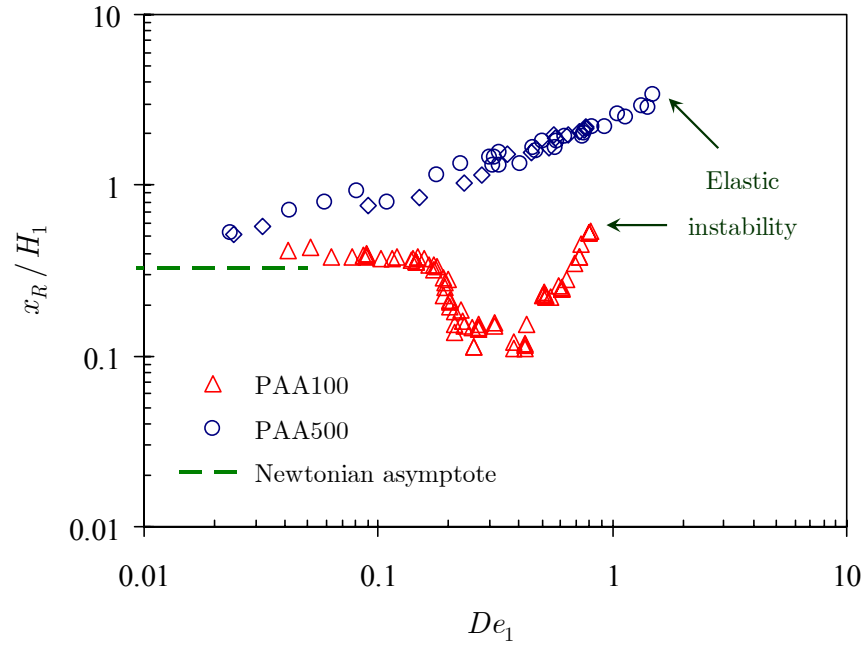


Fig. 10. Variation of normalised vortex length in the middle plane with the Deborah number for fluids PAA100 and PAA500.

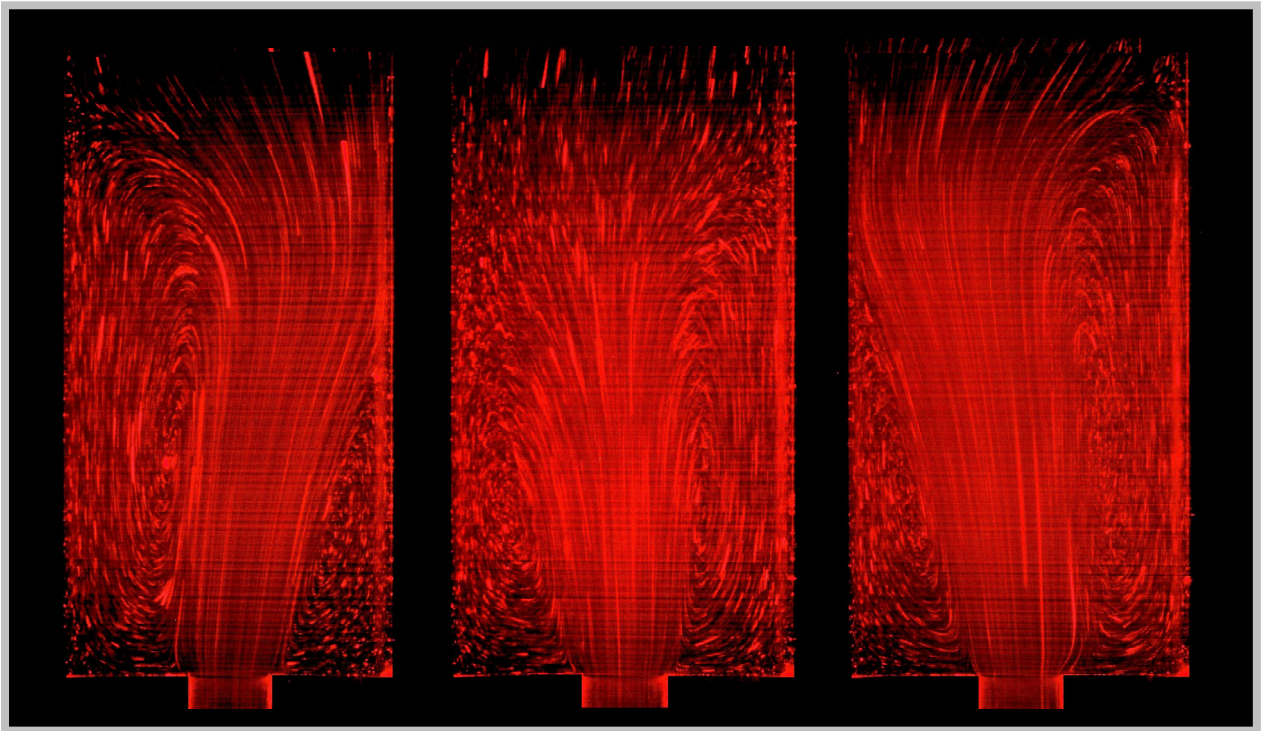


Fig. 11. Flow patterns for a super-critical shear rate for fluid PAA500 ( $De_1=1.94$  ;  $U_1 = 0.114$  cm/s).

#### ACKNOWLEDGEMENTS

The authors acknowledge funding by Feder via FCT programmes POCTI 37711/EME/2001 and POCTI 37699/EQU/2001. We are also grateful to Prof. M. P. Gonçalves and Mr. D. Torres of REQUIMTE, FEUP, for their help in characterizing the rheology of the fluids used in this work.

## REFERENCES

- Alves, M. A. (2004). "Escoamentos de fluidos viscoelásticos em regime laminar: análise numérica, teórica e experimental.", PhD thesis (in Portuguese), University of Porto, Portugal
- Alves, M. A., Pinho, F. T. and Oliveira, P. J. (2000). "Effect of a high-resolution differencing scheme on finite-volume predictions of viscoelastic flows", *J. Non-Newt. Fluid Mech.*, 93, pp. 287-314
- Bird, R.B., Armstrong, R.C. and Hassager, O. (1987). *Dynamics of polymeric liquids. Volume 1: Fluid Dynamics*, John Wiley & Sons, New York.
- Boger, D.V. (1987). "Viscoelastic flows through contractions", *Annual Rev. Fluid Mech.*, 19, pp. 157-182.
- Boger, D.V., Hur, D.U. and Binnington, R.J. (1986). "Further observations of elastic effects in tubular entry flows", *J. Non-Newt. Fluid Mech.*, 20, pp. 31-49.
- Boger, D.V., and Walters, K. (1993). *Rheological Phenomena in Focus*, Elsevier, Amsterdam
- Cable, P.J. and Boger, D.V. (1978a) "A comprehensive experimental investigation of tubular entry flow of viscoelastic fluids: Part I. Vortex characteristics in stable flow. *AIChEJ*, 24, pp. 868-879.
- Cable, P.J. and Boger, D.V. (1978b). "A comprehensive experimental investigation of tubular entry flow of viscoelastic fluids: Part II. The velocity fields in stable flow. *AIChEJ*, 24, pp. 992-999.
- Cable, P.J. and Boger, D.V. (1979). "A comprehensive experimental investigation of tubular entry flow of viscoelastic fluids: Part III. Unstable flow. *AIChEJ*, 25, pp. 152-159.
- Evans, R.E. and Walters, K. (1986). "Flow characteristics associated with abrupt changes in geometry in the case of highly elastic liquids" *J. Non-Newt. Fluid Mech.*, 20, pp 11-29.
- Hassager, O. (1988). "Working group on numerical techniques. Fifth International Workshop on Numerical Methods in Non-Newtonian Flows, Lake Arrowhead, USA" *J. Non-Newt. Fluid Mechanics*, 29, pp. 2-5.
- McKinley, G. H., Raiford, W. P., Brown, R. A. and Armstrong, R. C. (1991). "Non linear dynamics of viscoelastic flow in axisymmetric abrupt contractions", *J. Fluid Mechanics*, 223, pp 411-456.
- Nguyen, H. and Boger, D.V. (1979). "The kinematics and stability of die entry flows" *J. Non-Newt. Fluid Mech.*, 5, pp.353-368.
- Nigen, S. and Walters, K. (2002). "Viscoelastic contraction flows: comparison of axisymmetric and planar configurations" *J. Non-Newt. Fluid Mech.*, 102, pp. 343-359.79, pp. 1-43.
- Walters, K. and Rawlinson, D.M. (1982). "On some contraction flows for Boger fluids", *Rheol. Acta*, 21, pp. 547-552.
- Walters, K. and Webster, M.F. (1982). "On dominating elastico-viscous response in some complex flows", *Phil. Trans. R. Soc. London A*, 308, pp. 199-218.
- Xue, S., Phan-Thien, N. and Tanner, R. I. (1998). Numerical investigations of Lagrangian unsteady extensional flows of viscoelastic fluids in 3-D rectangular ducts with sudden contractions. *Rheol. Acta*, 37, pp. 158-169.